Fish and Shellfish Immunology 92 (2019) 450–459

Contents lists available at ScienceDirect

Fish and Shellfish Immunology

journal homepage: www.elsevier.com/locate/fsi

Full length article

Functional differentiation of three phosphatidylinositol 3-kinase catalytic subunit alpha (PIK3CA) in response to *Vibrio anguillarum* infection in turbot (*Scophthalmus maximus*)

Kai Zhang[a], Xiumei Liu[a,c], Miao Han[a], Yuxiang Liu[a], Xuangang Wang[a], Haiyang Yu[a], Jinxiang Liu[a,b], Quanqi Zhang[a,b,*]

[a] Key Laboratory of Marine Genetics and Breeding, Ministry of Education, Ocean University of China, Qingdao, 266003, China
[b] Laboratory for Marine Fisheries Science and Food Production Processes, Qingdao National Laboratory for Marine Science and Technology, Qingdao, 266237, China
[c] College of Life Sciences, Yantai University, Yantai, 264005, China

ARTICLE INFO

Keywords:
Scophthalmus maximus
PIK3CA
Expression profile
Single nucleotide polymorphism
Vibrio anguillarum-Resistance

ABSTRACT

PIK3CA has been extensively investigated from its molecular mechanism perspective and association with its mutations in different types of cancers. However, little has been reported regarding the pathological significance of PIK3CA expression in teleost. Here, in our present study, three PIK3CA genes termed *Sm*PIK3CAa, *Sm*PIK3CAb and *Sm*PIK3CA-like were firstly identified in the genome of turbot *S. maximus*. Although these three genes located in different chromosomes, all of them share the same five domains. Phylogenetic and synteny analysis indicated that *Sm*PIK3CAa, *Sm*PIK3CAb and *Sm*PIK3CA-like were three paralogs that may originate from duplication of the same ancestral PIK3CA gene. Subcellular localization analysis confirmed the cytoplasm distribution of these three paralogs. All three *Sm*PIK3CA were ubiquitously expressed in examined tissues in turbot, with the higher expression levels in immune-related tissues such as blood, spleen, kidney, gills and intestines. Upon *Vibrio anguillarum* challenge, *Sm*PIK3CAa and *Sm*PIK3CA-like transcripts were significantly induced in spleen, intestine and blood despite of differential expression levels and responsive time points. Additionally, individuals in resistant group showed significantly higher expression level of both two genes than in the susceptible group. Moreover, four SNPs (102, 2530, 3027 and 3060) and one haplotype (Hap2) located in exon region of *Sm*PIK3CA-like were identified and confirmed to be associated with *V. anguillarum* resistance in turbot by association analysis in different populations. Taken together, these results suggested that functional differentiation occurred in three *Sm*PIK3CA paralogs with *Vibrio anguillarum* resistance and *Sm*PIK3CAa and *Sm*PIK3CA-like probable play potential roles in innate immune response to pathogenic invasions in turbot.

1. Introduction

Phosphoinositol 3-kinases (PI3Ks) is an intracellular lipid kinase that phosphorylate the 3′-position of inositol ring to generate different phosphoinositides (PIs). In mammals, after responsing to a massive extracellular signaling polypeptides, PI3Ks are activated by receptor-associated kinase and then transduce signals to the downstream effector [1]. They also involved in a wide range of signaling pathways, such as PI3K/AKT pathway which related to proliferation, apoptosis, metabolism and immunity [2]. Accumulated evidence showed that activated PI3K/AKT pathway is currently considered integral to the innate immune response to pathogenic invasion in several organisms, including fish [3,4]. Depending on the substrate preference, PI3Ks were classified into three distinct classes (I, II and III) [5]. In Class I proteins, a heterodimer PIK3CA consisting of one catalytic subunit (p110α) and one regulatory subunit (p85) is considered to directly connected to cancer-cell growth in human [6]. In cancer, PIK3CA mutated or amplified at high rates in an array of tumor types [7]. The p110α isoform, encoded by PIK3CA, is expressed ubiquitously [8] and worked primary for proper growth-factor signaling and oncogenic transformation [9]. While PI3KCA proteins is well studied in human, little is known about this enzyme in other organisms, especially in non-mammals. PIK3CA was identified as an avian retrovirus-encoded oncogene that transforms chicken embryo fibroblasts [10]. In teleostean channel catfish (*Ictalurus punctatus*), PI3KCA was the most highly regulated gene under bacterial infection with *Edwardsiella ictaluri* and *Flavobacterium columnare*,

* Corresponding author. Key Laboratory of Marine Genetics and Breeding, Ministry of Education, Ocean University of China, No.5 Yushan Road, Qingdao, 266003, China.
E-mail address: qzhang@ouc.edu.cn (Q. Zhang).

https://doi.org/10.1016/j.fsi.2019.06.035
Received 14 March 2019; Received in revised form 12 June 2019; Accepted 13 June 2019
Available online 14 June 2019

showing immune functions in pathogenic invasion [11]. Finally, a recent study presents the impact of PI3K on the fish blood immunity in Japanese flounder (*Paralichthys olivaceus*) [12].

The turbot, *Scophthalmus maximus*, is an economically important marine fish species cultured widely in China since introduced from Europe in last two decades [13]. Turbot industry encountered great challenges including devastating diseases which cause large economic losses. Many studies have been conducted to explored effective approaches to preventing diseases, such as drug screening and vaccine development [14,15]. However, considered the vaccine titer and cost of cultivation, genetic breeding may be more effective and sustainable. Thus far, several successful cases have been reported for disease control in vertebrates and invertebrates in breeding programs with marker-assisted selection (MAS) [16,17]. As a Gram-negative bacteria, *Vibrio anguillarum* can target many aquatic animals and cause serious episodes, particularly in teleost [18]. In a previous study, seven SNPs located on different genes were identified to be associated with *Vibrio anguillarum* resistance [19]. Among these genes, PIK3CA-like gene attracted our attention for its unique expression pattern.

In this study, three homologous *Sm*PIK3CA initially were identified from the genome of turbot. We conducted phylogenetic and synteny analyses of vertebrate PIK3CA genes. Then, comparisons of expression pattern and subcellular localization of the three PIK3CA genes in turbot were performed. The result revealed probable sub-function of *Sm*PIK3CAa and *Sm*PIK3CA-like. This study lays the foundation for evolutionary and functional studies of the PIK3CA gene in teleost. We also provide basic information for functional analysis of *Sm*PIK3CA-like SNPs in *S. maximus*, and implied that the *Sm*PIK3CA-like SNPs could be used as potential markers for selective breeding of turbot with *Vibrio anguillarum* resistance.

2. Materials and methods

2.1. Fish, bacterial challenge and ethics statement

Healthy one-year-old turbot (average mass of 136 g) were obtained from Haiyang Yellow sea aquatic product CO., Ltd, Shandong, China. Before *V. anguillarum* challenge, the fish were kept in aerated fresh seawater at 19 °C for three days for acclimatization. Water was replaced once daily. The turbot was not subjected to any further study until no abnormal symptom was observed. For the bacterial challenge experiment, 220 individuals (population 17) were intraperitoneally injected with *V. anguillarum* (3×10^8 CFU) at a dose of 1 μL/g of fish weight, whereas the control group (5 individuals) were injected with Ringer's solution for marine teleost in same way. During 24 h after injection, fish were died with classical *V. anguillarum* clinic signs. 192 individuals were divided into the *Vibrio*-resistant group (17-R) and the susceptive group (17-S) according to their survived time (17-R: n = 96; 17-S: n = 96).

An independent turbot population (population 18, 100 individuals, 1.5-year-old, average mass of 350 g) was used to certify SNPs associated with *V. anguillarum*-resistant. Population 18 was consisted of 5 full-sib families with 20 individuals each. The injected doses of *V. anguillarum* was the same with previously experiment. After challenge, the first 35 dying individuals with obvious *V. anguillarum* clinic infection symptom were collected as susceptible individuals. Seven days of the challenge later, all survived fish were collected as resistant fish from which 35 individuals were selected randomly to build resistant individuals.

All animal experiments were conducted in accordance with the Institutional Animal and Use Committee of the Ocean University of China and the China Government Principles for the Utilization and Care of Vertebrate Animals Used in Testing, Research, and Training (State Science and Technology Commission of the People's Republic of China for No. 2, October 31, 1988. http://www.gov.cn/gongbao/content/2011/content_1860757.htm).

2.2. DNA extraction, RNA isolation, and cDNA synthesis

The dorsal muscle of each turbot from the population 17 was removed and kept at −80 °C for DNA extraction. Genomic DNA was extracted through phenol/chloroform procedure [20]. The heart, liver, spleen, kidney, brain, gill, muscle, intestine and blood were collected from three uninfected fish and homogenised in TRIzol reagent (Invitrogen, USA) to obtain the total RNA following the manufacturer's instructions. RNA was obtained from these tissues for analysis of tissue distribution. In addition, the liver, gill, intestine and blood samples were isolated from three injected fish at 0–72 h post-infection (hpi). RNA from these tissues was obtained to analyse the response of the three PI3KCA genes to *V. anguillarum* infection. For gene expression comparison in resistant and susceptive group, the liver, spleen, kidney, gill, intestine and blood samples were collected from three resistant individuals and three susceptible individuals. Genomic DNA and total RNA were detected by agarose gel electrophoresis and Nanophotometer Pearl (Implen GmbH, Germany) for quality and quantity. Then, total RNA was reversed using the Reverse Transcriptase M-MLV System (TaKaRa, China).

2.3. cDNA cloning and bioinformatics assay

The open reading frame (ORF) of three PIK3CAs were obtained from the genome of *S. maximus* (PRJEB11743) [21]. Specific primers (Table S1) were designed according to their deduced cDNA sequences extracted from the genome. The cDNA of *S. maximus* gills was used as template for PCR amplification. PCR products were separated by 1.5% agarose gel electrophoresis, purified using a Zymoclean Gel DNA Recovery Kit (Zymo Research, Orange, CA, USA), cloned into the pMD-19T (simple) vector (Takara, Dalian, China) and sequenced.

The conserved domains were predicted using the SMART (http://smart.embl-heidelberg.de/smart/set_mode.cgi) online tool. The cDNA sequences were aligned by GSDS 2.0 to predict exon/intron boundaries [22]. Multiple sequence alignments were performed by the Clustal X 2.1 (http://www.ebi.ac.uk/tools/clustalw2.1). A Bayesian phylogenetic tree was constructed using MrBayes 3.2.6 [23]. For Bayesian analysis, 200,000 generations of MCMC were performed. All other options and priors were the default settings of MrBayes 3.2.6 software. GenBank accession numbers of the PI3K protein sequences mentioned above are listed in Supplementary Table 2.

2.4. Syntenic analysis

The homologies of the PI3KCAs, and their neighboring genes in turbot, were examined through comparing those among tetrapod and marine teleost, to provide additional evidence for gene identification and orthology. All data was extracted from genome databases at the National Center for Biotechnology Information, Ensembl or Genomicus (version 82.01) [24]. BLASTP was used to annotate these neighboring genes by searching against NCBI database.

2.5. Expression profile of genes in normal and challenged organs

Real-time PCR assays were conducted to examine the expression of *Sm*PIK3CAa, *Sm*PIK3CAb and *Sm*PIK3CA-like in major organs of turbot. Specific primers (Table S1) were designed across exon-3′UTR borders to avoid amplification of other homologous genes. q-PCR were implemented using NovoStart SYBR qPCR Super MIX (Novoprotein Scientific Inc.) following the methods described by Liu et al. [17]. β-actin was used as the reference gene. The expression levels of all the target genes were calculated by the $2^{-\Delta\Delta Ct}$ method [25].

2.6. Plasmids construction

The full length of ORFs of three *Sm*PIK3CA genes was cloned into

the pEGFP-N1 vector containing a C-terminal GFP tag with specific primers (Table S1). Finally, the recombinant plasmids were cleaved by restriction enzymes and verified by DNA sequencing, and designated, pEGFP-N1-*Sm*PIK3CAa, pEGFP-N1-*Sm*PIK3CAb and pEGFP-N1-*Sm*PIK3CA-like, respectively.

2.7. Cell culture, transient transfection and subcellular localization

Human embryonic kidney 293T (HEK293T) cells were used for the subcellular localization analysis. Cells were cultured in Dulbecco's modified Eagle's medium (DMEM, Gibco, USA) supplemented with 10% fetal bovine serum (FBS, Gibco BRL) and antibiotics (100 mg/L streptomycin and 105 U/L penicillin, Gibco) in a humidified atmosphere of 95% air and 5% CO_2 at 37 °C.

For DNA transfection, dissociated HEK293T cells were added to 12-well cell culture plates (approximately 2×10^5/well) and cultured for 8 h at 37 °C. Then, they were transfected with the plasmids described previously (1000 ng/well) using the LipoGene™ 2000 PLus Transfection Reagent (US Everbright Inc.) when the cells were 70–80% confluent according to the manufacturer's instructions. pEGFP-N1 was used as control for transfection. After 24 h, the cells were fixed with 4% paraformaldehyde for 20 min and washed with PBS 3 times. Then, the cells were stained with DAPI (Beyotime, China) for 20 min to visualize the nuclei and followed by washing three times. Finally, images of the fluorescent protein expression were collected using a laser scanning confocal microscopy.

2.8. SNPs selection, genotyping and validation

The SNPs of *Sm*PIK3CA-like were predicted based on the whole genome resequencing data sets (PRJNA512430). According to annotations, all SNPs in the exon region were picked out. SNPs with quality score higher than 20 were chosen for further analysis.

Selected SNPs were genotyped in population 17 using Fluidigm EP1 KASP (The Kompetitive Allele Specific PCR genotyping) system. The primers used for genotyping were shown in Table S1. The detailed processes could be identified in Wang' study [26]. At last, 220 individuals were genotyped to take Hardy-Weinberg equilibrium (HWE) and minor allele frequency (MAF) analyses. The results of genotype from 17-S and 17-R were used to determine the SNPs associated with *V. anguillarum*-resistance. Seventy individuals (35 susceptible individuals and 35 resistant individuals) from population 18 were genotyped by PCR and sequenced with the primer *Sm*PIK3CA-like-verify 1 and 2 to validate the SNPs and haplotypes.

2.9. Statistical analysis

One-way ANOVA with Tukey's test was used to analyse *Sm*PIK3CAs mRNA expression in different samples, which was performed using SPSS 20.0 software (IBM, New York, USA). Data were considered significantly different when $P < 0.05$. All data are presented as mean ± standard error of mean (SEM).

Allele frequencies of each SNP locus from different turbot populations were calculated. The SNP loci with minor allele frequency (MAF) less than 5% in all populations were discarded. Hardy-Weinberg equilibrium (HWE) of was tested using Pearson's Chi-square test in SPSS 20.0 software. The SNP loci deviating from HWE ($P < 0.05$) were discarded. The *V. anguillarum*-resistance association analysis was performed by Pearson's Chi-square test in SPSS 20.0. The haplotype structure and linkage disequilibrium (LD) were analyzed with Haploview 4.2 software. The associations between haplotypes and *V. anguillarum*-resistance were detected using SHEsis software [27].

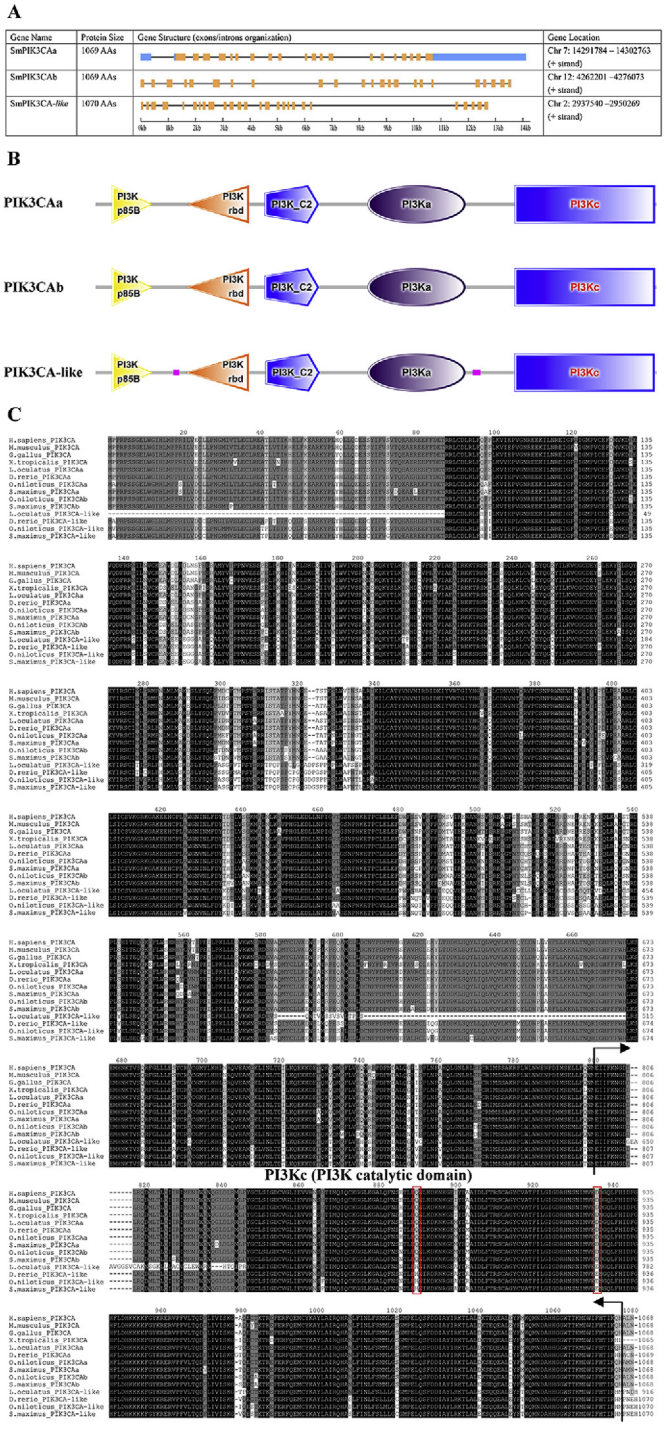

Fig. 1. Characterization of *Sm*PIK3CAa, *Sm*PIK3CAb and *Sm*PIK3CA-like. (A) Gene loci and gene structures. Exons/introns organization is represented by different colors. (B) Protein structure of three *Sm*PIK3CA genes. Gray stripe indicates the ORF region. Domain organization of genes is represented by different colors. PI3K p85B: PI3-kinase family, p85-binding domain; PI3K rbd: PI3-kinase family, Ras-binding domain; PI3K C2: Phosphoinositide 3-kinase, region postulated to contain C2 domain; PI3Ka: Phosphoinositide 3-kinase family, accessory domain and PI3Kc: Phosphoinositide 3-kinase, catalytic domain. (For interpretation of the references to color in this figure legend, the reader is referred to the Web version of this article.) (C) Multiple alignment analysis of PI3KCA protein homologues from both invertebrates and vertebrates. Similar amino acid residues are labeled in gray while uniform amino acid residues are labeled in black. The conserved PI3K catalytic domain is shown with arrows. Some amino acid changes are marked with red boxes.

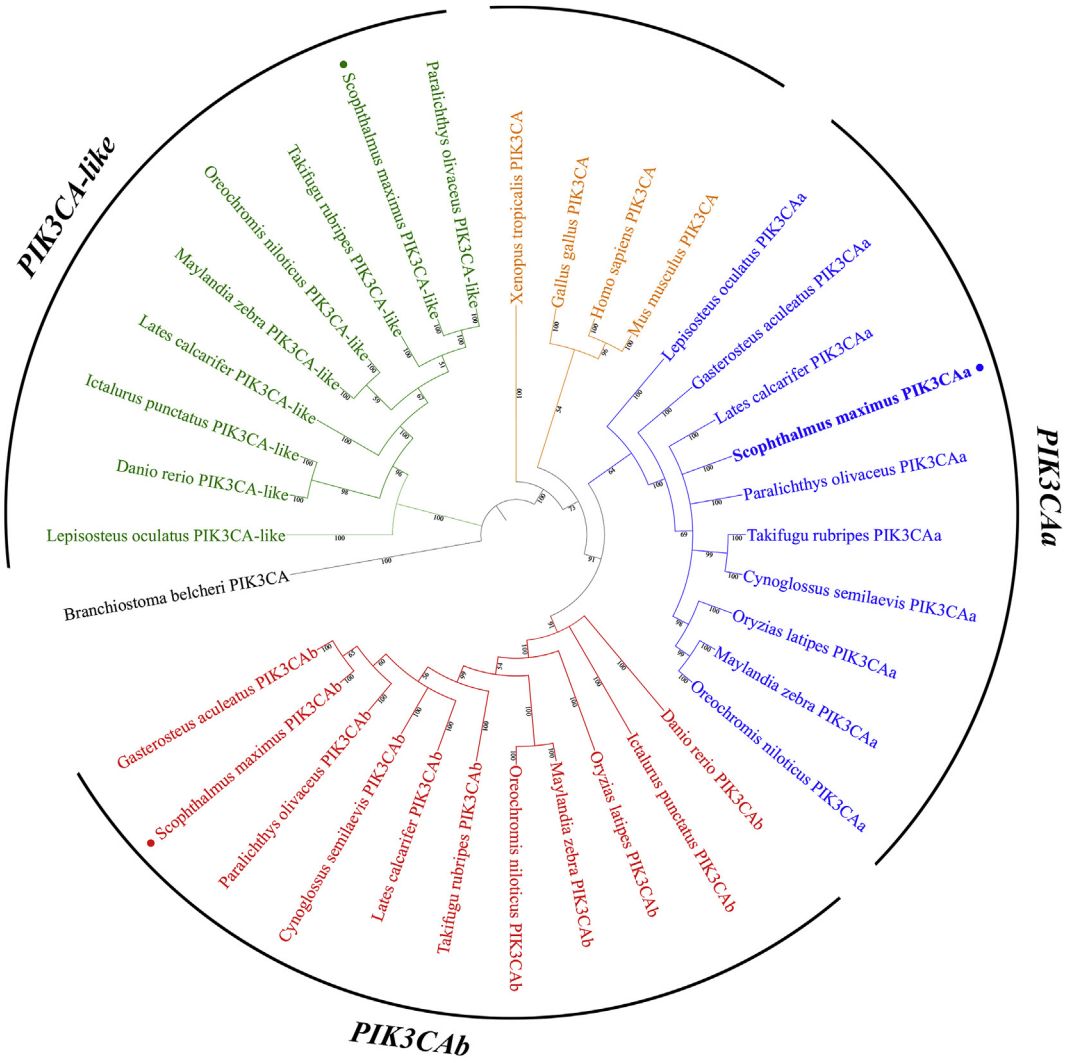

Fig. 2. Bayesian phylogenetic tree based on three full *Sm*PIK3CA amino acid sequences of 17 species. The species of *S. maximus* is highlighted with points. mcmc = 200,000 generations. The accession numbers of genes from other species were provided in Supplementary File Table S2.

3. Results

3.1. Three PIK3CA paralogs present in the S. maximus genome

Three PI3KCA genes, *Sm*PIK3CAa, *Sm*PIK3CAb and *Sm*PIK3CA-like, were identified through the homologous alignment of the *S. maximus* genome. The complete nucleotide sequences and the deduced amino acid sequences of *Sm*PIK3CAa, *Sm*PIK3CAb and *Sm*PIK3CA-like were submitted to the NCBI database (accession numbers MK625172, MK625173 and MK625174), encoding proteins of 1069, 1069 and 1070 AAs, respectively (Fig. 1A). All three genes are located on different chromosomes. *Sm*PIK3CAa and *Sm*PIK3CAb are distributed on Chr 7: 14291784–14302763 and Chr 12: 4262201–4276073, while *Sm*PIK3CA-like is located on Chr 2: 2937540–2950269. As the results of DNA structure prediction, genomic organization of these three *Sm*PIK3CA genes is not exactly similar. *Sm*PIK3CAa consist of 20 exons and 19 introns and *Sm*PIK3CAb contains 23 exons and 22 introns. Different with that two genes, *Sm*PIK3CA-like has more exons, reaching 26. Moreover, it also contains an intron of more than 5k bp, which is not found in the other two genes.

Like mammals, the putative proteins of these three PIK3CAs possessed all domains including PI3K p85B, PI3K rbd, PI3K C2, PI3Ka, and PI3Kc domains (Fig. 1B). Multiple alignment analysis revealed that all three genes share high similarity in five domains, especially in the PIK3c domain (Fig. 1C). We also found amino acid changes in orientation of PIK3CA-likes in examined fishes.

3.2. Phylogenetic reconstruction and syntenic analysis

To elucidate the molecular evolutionary relationships of all studied proteins between *S. maximus* and other species, a Bayesian phylogenetic tree was constructed based on their corresponding amino acid sequences obtained from teleost fish and non-fish. As shown in Fig. 2, the PI3KCAs of various species were clearly clustered into four clades consisting of teleostean and mammalian branches. PIK3CA proteins could be divided into three groups: PIK3CAa group, PIK3CAb group and PIK3CA-like group. Two PIK3CAs homologues from spotted gar (*Lepisosteus oculatus*) fell in PIK3CAa group and PIK3CA-like group, respectively. Unlike spotted gar, two genes from zebrafish (*Danio rerio*) were grouped in PIK3CAb group and PIK3CA-like group, respectively. *Sm*PIK3CAa and *Lo*PIK3CA had a closer relationship in the phylogenetic tree. Additionally, *Sm*PIK3CAb showed the closest evolutionary relationship with the *Dr*PIK3CA.

As shown in Fig. 3, the PIK3CA genes and the surrounding genes were mapped according to their relative locations on the same chromosome or scaffold. A conserved syntenic relationship was detected among the PIK3A genes from human (*Homo sapiens*), mouse (*Mus musculus*), chicken (*Gallus gallus*) and spotted gar. In other teleost

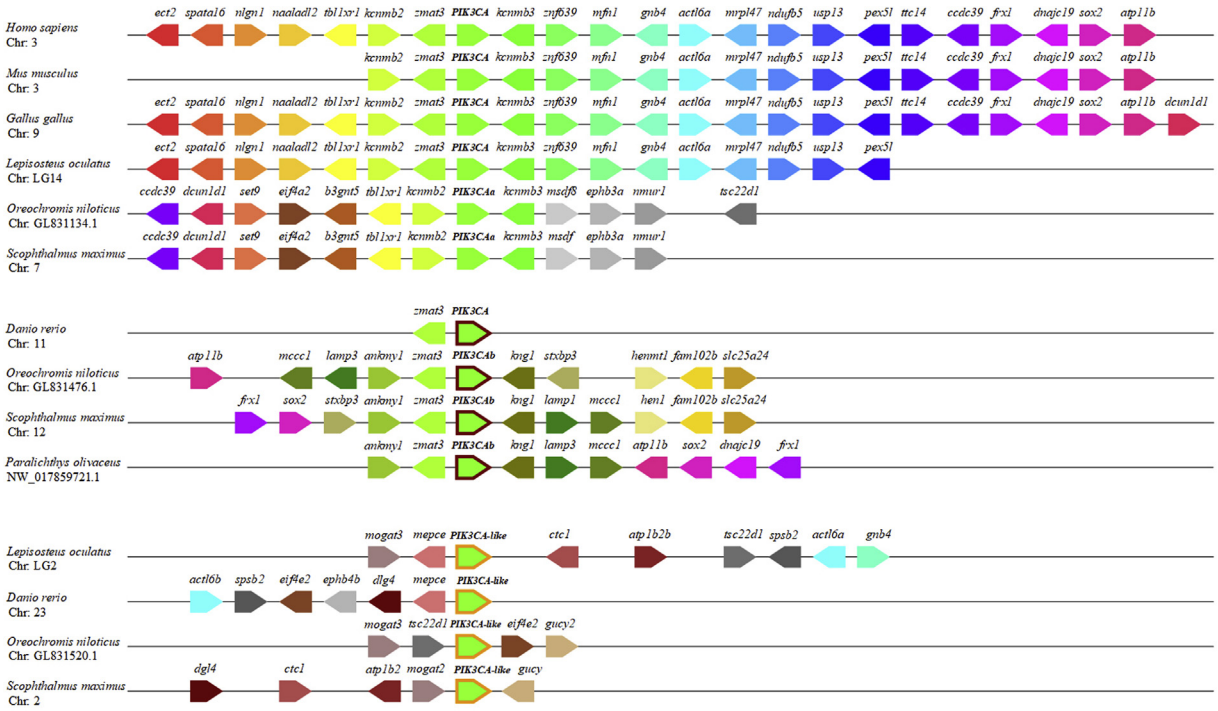

Fig. 3. Syntenic analysis of PIK3CA genes in vertebrates. Sequences used in the analysis included genomic neighborhood containing PIK3CA related genes from human, mouse, chicken, spotted gar, zebrafish, channel catfish and turbot. The arrows in different colors stand for different genes and the arrowheads point in the direction of the corresponding gene. Gene order was determined according to their relative positions in the same chromosome or scaffold. (For interpretation of the references to color in this figure legend, the reader is referred to the Web version of this article.)

examined in this study, the genomic neighborhood regions surrounding PI3K3CAa genes are displayed and it is also conserved. In contrast, the surrounding genes of PIK3CAb from tilapia (*Oreochromis niloticus*) and turbot changed a lot compared with the syntenic genes of PIK3CAa. Only the orthologous gene of *zmat3* was retained and others were changed or deleted. In PIK3CA-like genes from four teleost (*L. oculatus*, *D. rerio*, *O. niloticus* and *S. maximus*), the upstream and downstream genes were found to have changed through evolution. Several genes were found to have moved, lost and shifted. Although the syntenic relationship of PIK3CA-like was not consistent among those species, regularities also could be discovered. The orthologs of gene *mogat* were located in the same chromosome as PIK3CA-like and they often situated close to PIK3CA-like. Therefore, the separate grouping of PIK3CA homologues of examined fishes indicating that a gene duplication event of PIK3CA may have took place in the common ancestor of all extant teleosts.

3.3. Tissue distribution and temporal expression profile of SmPIK3CA genes following bacterial challenge

Quantitative real-time PCR results indicated that PIK3CAa, PIK3CAb and PIK3CA-like showed differential tissue-specific expression pattern in turbot. All three genes were ubiquitously expressed in all nine examined organs (heart, liver, spleen, kidney, brain, gill, muscle, intestine and blood) (Fig. 4). The expression of the *Sm*PIK3CAa was found to be predominantly in the blood (5.5-fold compare to muscles), followed by spleen (3.7-fold compare to muscles) and heart (3.1-fold compare to muscles) (Fig. 4A). The highest level of the *Sm*PIK3CAb was also observed in blood (8.4-fold compare to muscles) (Fig. 5B), while *Sm*PIK3CA-like was remarkably expressed in spleens (8.8-fold compare to muscles) (Fig. 4C). Despite of the spleens, *Sm*PIK3CA-like was also obviously expressed in blood, livers, gills and intestines (7.7-, 5.6-, 5.6- and 5.1-fold compared to muscles, respectively) (Fig. 4C). All three PIK3CAs had the lowest mRNA expression levels in muscles tissues in comparison.

Temporal expression of *Sm*PIK3CAa, *Sm*PIK3CAb and *Sm*PIK3CA-like upon stimulations with *V. anguillarum* in four tissues (spleen, gill, intestine and blood) were investigated. As shown in Fig. 5, *Sm*PIK3CAa, *Sm*PIK3CAb and *Sm*PIK3CA-like transcriptions were induced upon *V. anguillarum* stimulations. The expressions of the *Sm*PIK3CAa were up-regulated after the challenge in the three immune organs reaching the peaks at 12 h in spleen and intestine, and at 6 h in blood (Fig. 5A). The peak levels of the *Sm*PIK3CAa reached 3.3-fold in spleen and 3.1-fold in intestine compared the control one. The least levels of the *Sm*PIK3CAa were noticed both at 3 h in all four tissues. Similarly, the expression levels of the *Sm*PIK3CA-like were also drastically elevated after *V. anguillarum* stimulation, with the peaks appeared at 1 h in spleen and gill, and at 6 h in intestine and blood (Fig. 5C). After that, the *Sm*PIK3CA-like transcription decreased from 6 h to 72 h showing negatively regulation. Compared with these two genes, the expressions of *Sm*PIK3CAb mRNA showed volatility expression pattern and reached a in a significant level at 72 h in spleen and intestine (Fig. 5B). No significant inductions of PIK3Cab examined in any time points in gill and blood. Overall, *Sm*PIK3CAa and *Sm*PIK3CA-like showed a similar expression pattern in the spleen, intestine and blood; that is, the expression levels of these two genes were quickly upregulated before 12 h and gradually decreased until 72 h *Sm*PIK3CA-like transcription was induced even earlier than *Sm*PIK3CAa. *Sm*PIK3CAb had no regularity expression pattern.

At last, the mRNA expression profile of *Sm*PIK3CAa, *Sm*PIK3CAb and *Sm*PIK3CA-like in different organs of susceptible individuals and resistant individuals relied on qPCR. The relative expression level of *Sm*PIK3CAa was higher in resistant group than in susceptible group in spleen, kidney, intestine and blood ($P < 0.05$) (Fig. 6A). Similar results were found in *Sm*PIK3CA-like expression patterns with kidney replaced by gill (Fig. 6C). In intestine, difference of *Sm*PIK3CA-like between the two groups reached upon to 17.3-fold. However, no difference was detected for the expression level of *Sm*PIK3CAb between these two groups (Fig. 6B). These results indicated that *Sm*PIK3CAa and *Sm*PIK3CA-like was up-regulated in immune organs in resistant group

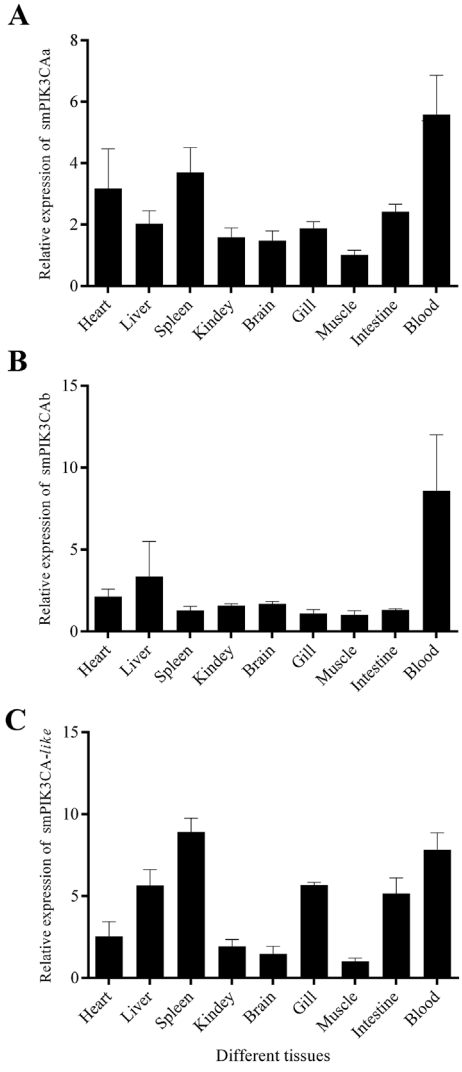

Fig. 4. Tissue distributions of *Sm*PIK3CAa (A), *Sm*PIK3CAb (B) and *Sm*PIK3CA-like (C). The variance of this expression was represented as a ratio (the amount of *Sm*PIK3CAa, *Sm*PIK3CAb and *Sm*PIK3CA-like mRNA normalized to the corresponding reference gene values). Data are shown as mean ± SD (n = 3).

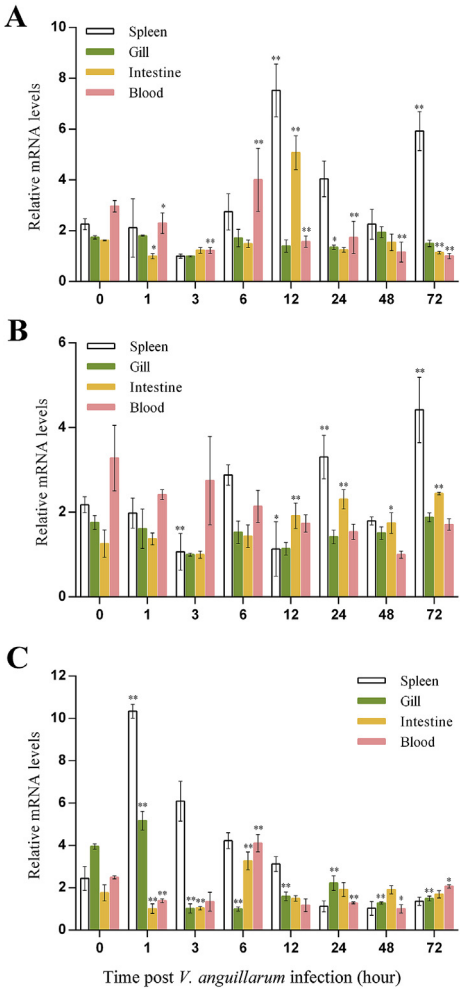

Fig. 5. Expression level of three PIK3CA genes in *S. maximus* after *V. anguillarum* infection. (A) *Sm*PIK3CAa, (B) *Sm*PIK3CAb and (C) *Sm*PIK3CA-like. RNA was isolated from spleen, gill, intestine and blood, and subjected to qPCR. β-Actin gene expression was used as an internal control. Vertical bars represent the mean ± SE (N = 3). Asterisks '**' and '*' indicate statistical significance of $P < 0.01$ and $P < 0.05$, respectively.

after *V. anguillarum* challenge.

3.4. The three PIK3CAs have same subcellular localizations

HEK293T cells were transfected with plasmids encoding GFP-tagged *Sm*PIK3CAa, *Sm*PIK3CAb and *Sm*PIK3CA-like to detect their subcellular localization. As is shown in Fig. 7, a clear fluorescent signal was observed under the microscope and all three *Sm*PIK3CA recombinant proteins were dominantly distributed in the cytoplasm. Thus, the consistency of *Sm*PIK3CA by subcellular localization tentatively suggested the three genes are not evolved completely in functions.

3.5. SNPs and haplotypes in SmPIK3CA-like associated with V. anguillarum resistance

Ten SNPs were discovered in the CDS region of *Sm*PIK3CA-like from previous data of our laboratory. At last, a total of 220 individuals from 17 population were used for genotyping. After general statistical analysis and Chi-square test, of these SNPs, 10 SNPs were common (MAF > 5%), and only 7 SNPs were applied to the association analysis after HWE analysis (Table S3). The location of each SNP was relative to the transcriptional start (ATG).

Genotypes and allele frequencies of the 7 selected SNPs were shown in Table 1. The results indicated that 4 SNPs (102, 2530, 3027 and 3060) were significantly associated with *V. anguillarum* resistance both in genotypes and alleles. Among the 4 SNPs, one is nonsynonymous and the other three are synonymous.

The linkage disequilibrium (LD) pattern based on these four candidate SNPs was characterized, and three haplotypes were obtained. As shown in Fig. 8, SNP 3027 and 3060 were strongly linked (D' > 0.9). Two *V. anguillarum* resistance-associated haplotypes were identified by comparing haplotype frequencies between the 17-S and 17-R (Table 2). In detail, the haplotype frequencies of Hap1 (CC) were significantly higher in the 17-S group than those in the 17-R group ($P < 0.01$), which indicated that Hap1 might increase the risk of *V. anguillarum* infection. In contrast, the frequencies of Hap2 (TT) were significantly lower in the 17-S group than those in the 17-R group ($P < 0.01$), suggesting that Hap2 was a protective haplotype.

3.6. Validation of SNPs and haplotypes

To verify *V. anguillarum* resistance-associated SNPs identified based on 17-R and 17-S, seventy individuals of *S. maximus* from 18-R and 18-S were used for SNP genotyping. The genotype and allele frequencies of

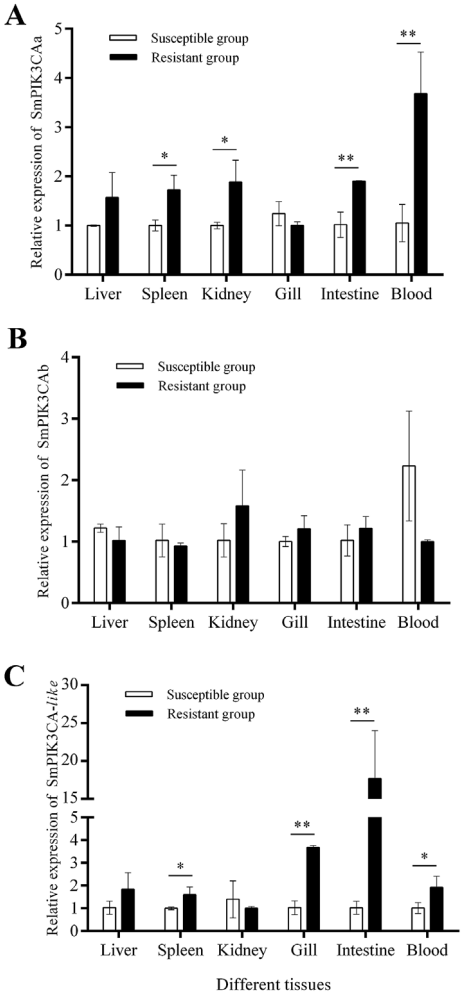

Fig. 6. Expression profiles of *Sm*PIK3CAs transcription in different groups upon *V. anguillarum* challenge. (A) *Sm*PIK3CAa, (B) *Sm*PIK3CAb and (C) *Sm*PIK3CA-like. The variance of this expression was represented as a ratio (the amount of *Sm*PIK3CAa, *Sm*PIK3CAb and *Sm*PIK3CA-like mRNA normalized to the corresponding reference gene values). Data are shown as mean ± SD (n = 3). Asterisks '**' and '*' indicate statistical significance of $P < 0.01$ and $P < 0.05$, respectively.

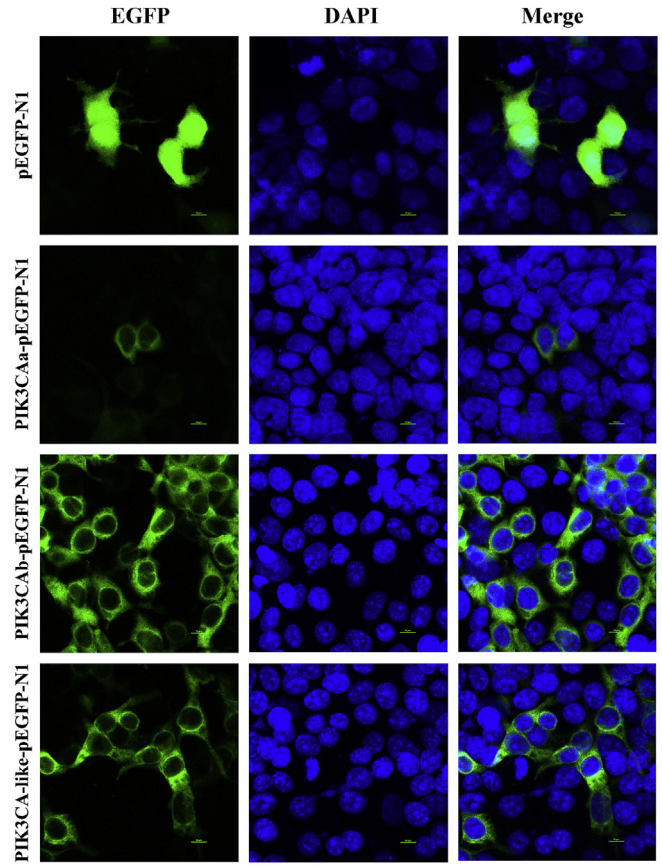

Fig. 7. Subcellular localization of three *Sm*PIK3CA genes in HEK293T cells. The left-hand panels depict GFP staining, the middle panels depict DAPI staining, and the right-hand panels depict merged DAPI/GFP staining. The upper panels depict localization of the GFP negative control, and the 2–4 panels depict localization of the *Sm*PIK3CAa-pEGFP-N1, *Sm*PIK3CAb-pEGFP-N1 and *Sm*PIK3CA-like-pEGFP-N1 proteins.

SNP 102, 2530, 3027 and 3060 were shown in Table 3. The genotype and allele frequencies of the four SNP were both significantly different between population 18-R and 18-S, which indicated that SNP 102, 2530, 3027 and 3060 contributed to the genetic basis of *V. anguillarum* resistance. We also calculated the frequencies of Hap1 and Hap2. As listed in Table 4, the haplotype frequency of Hap2 between population 18-R and 18-S was consistent with population 17-R and 17-S, which confirmed that Hap2 was a protective haplotype.

4. Discussion

Mutations in PIK3CA are known to activate the PI3K/AKT pathway which involved in many physiological processes, including cell proliferation, apoptosis and protein synthesis [28]. Furthermore, numerous studies indicate that this pathway plays a pivotal role in innate immune system [29,30]. Although well studied in mammalian species, the knowledge of PIK3CA in teleost is deficit. Therefore, we focused on the molecular characterization and expression profile of PIK3CA genes in *S. maximus*.

Computer models predicted that all three PI3KCAs possessed the domain topology containing five domains. Multiple-sequence alignment showed that the PI3Kc domain, which possessed the ATP-binding sites, has the highest identity with PI3KCA from other species implying that all the three *Sm*PIK3CAs may exert similar biological functions with other species reported. It has been demonstrated that the PI3K p85B domain and PI3Kc domain act a pivotal part in inflammatory responses, vesicle trafficking and secretion, and apoptosis [31]. However, amino acid changed were observed at specific sites in PIK3CA-like genes, i.e. His replaced the Gln in PI3Kc domain. The underlying basis behind this scenario remains unclear and needs to be further research. Taken together, the presence of conserved domains suggested that *Sm*PIK3CAa, *Sm*PIK3CAb and *Sm*PIK3CA-like genes could be considered as essential component of host defense that is involved in innate immune responses in *S. maximus* as their correspondents acted in mammals.

A plenty of PIK3CA orthologs were retrieved to construct the phylogenetic tree to elucidate the phylogenetic status of three *Sm*PIK3CA genes. Annotation of these genes was relatively straightforward (Fig. 3). All PIK3CA orthologs grouped separately to form PIK3CAa clade, PIK3CAb clade and PIK3CA-like clade, respectively, before clustered together. Among which, the PIK3CAa and PIK3CAb clusters has more close relationship with PIK3CA proteins in tetrapodas. As is well known, spotted gar (a nonteleost ray-finned fish) lineage diverged from teleosts before the TGD and its genome is organized more similarly to that of humans than teleosts [32]. The two paralogs of PIK3CA from spotted gar were clustered into PIK3CAa and PIK3CA-like clade suggesting that a gene duplication event of PIK3CAa and PIK3CAb may have occurred in the ancestor of bone fish. The PIK3CA sequence from zebrafish which fell in PIK3CAb and PIK3CA-like clade also confirmed this view. Moreover, genomic regions with the relevant genes were

Table 1
Association analysis of single SNPs associated with V. anguillarum-resistance.

Code	Location	Genotype	Count (frequence)		ChiSq genotype	ChiSqAllele	*P value*	
			17-S	17-R			ProbGenotype	ProbAllele
1	102	CC	60(0.625)	38(0.409)	8.979	7.175	0.011*	0.007**
		CT	27(0.281)	43(0.462)				
		TT	9(0.094)	12(0.129)				
2	405	GG	46(0.500)	43(0.457)	0.432	0.164	0.806	0.685
		GA	33(0.359)	38(0.404)				
		AA	13(0.141)	13(0.138)				
3	1050	CC	28(0.298)	35(0.368)	1.084	1.048	0.582	0.306
		CT	42(0.447)	39(0.411)				
		TT	24(0.255)	21(0.221)				
7	2530	GG	13(0.138)	27(0.281)	6.399	6.352	0.041*	0.012*
		GA	42(0.447)	40(0.417)				
		AA	39(0.415)	29(0.302)				
8	2817	TT	20(0.213)	16(0.174)	1.103	0	0.576	0.988
		TG	47(0.500)	53(0.576)				
		GG	27(0.287)	23(0.250)				
9	3027	CC	59(0.634)	36(0.387)	11.393	10.69	0.003**	0.001**
		CT	26(0.280)	43(0.462)				
		TT	8(0.086)	14(0.151)				
10	3060	CC	30(0.316)	9(0.095)	14.246	9.58	0.001**	0.002**
		CT	40(0.421)	52(0.547)				
		TT	25(0.263)	34(0.358)				

Superscript (*) and (**) indicate significant difference at the $P < 0.05$ and $P < 0.01$ level, respectively.

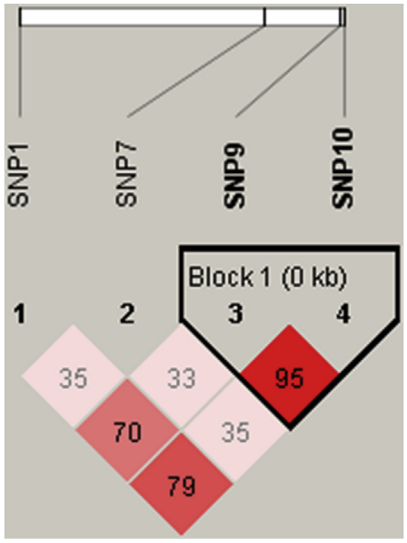

Fig. 8. LD structure among the 4 SNPs of *Sm*PIK3CA-like in 17-R and 17-S. One LD blocks are circled, which were derived using Haploview 4.2 software. The D', a measure of LD, is the correlation coefficient between pairs of SNP loci. The numbers in red boxes represent the values of the D' and the number is absent when the value equals 1. (For interpretation of the references to color in this figure legend, the reader is referred to the Web version of this article.)

retrieved and syntenic analysis was conducted. From the conserved syntenies, the duplicated genes of PIK3CA were derived from TGD (Fig. 4) for the reason that no duplications of PI3K genes were observed in mammals, birds, amphibians, or reptiles. In addition, the presence of duplicated PIK3CA genes on different chromosomes or LGs is another powerful evidence, which is consistent with the study of Li et al. [11].

In mammalians, PI3K has been found in the cytosol, from where it is recruited to the membrane once receptors are activated [33]. In our study, the results of subcellular localization showed that all three *Sm*PIK3CA genes were located in the cytoplasm of HEK293T cells. This distributions of *Sm*PIK3CAs corresponds to its putative function that PI3K transduces cellular responses in cytoplasm. Moreover, in aquatic animals, the AKT also distributed in the cytoplasm which implies that PIK3CA could be involved in the AKT regulation, thus activating immune-related gene expression [34,35].

The tissue distribution analysis showed ubiquitous expression profiles of all three *S. maximus* PIK3CA in all nine examined organs, indicating a versatile functional role in the physiological activities of turbot. However, the *Sm*PIK3CAa and *Sm*PIK3CA-like were both highly expressed in the immune-related organs, such as liver, spleen, kidney, gill, intestine and blood. Similar results were also reported in aquatic animals, i.e. PIK3CA were highly expressed in gill in channel catfish [11]. It has been reported in Japanese flounder that haemocytes is one of the major immune tissues recognizing and eliminating bacterial pathogens [12]. The gills in goldfish (*Carassius auratus L.*) constantly exposed to external environment and formed the first defense barrier to contract with pathogenic microorganisms [36]. In contract, the liver and spleen are expected to be the last barrier once the pathogen

Table 2
Association between SmPIK3CA-like haplotypes and V. anguillarum-resistance in 17-R and 17-S#.

Variables	Haplotype	Frequency			Chi square values	*P value*	OR (95%CI)
		All	17-S	17-R			
Hap1	CC	0.439	0.526	0.349	13.206	< 0.001**	0.461 (0.303, 0.702)
Hap2	TT	0.299	0.231	0.366	9.956	< 0.001**	2.073 (1.313, 3.272)
Hap3	CT	0.255	0.242	0.271	0.68	0.409	1.218 (0.762, 1.949)

Haplotypes with frequencies < 0.05 were not included in the table; OR: odds ratio; CI: 95% percent confidence interval; Superscript (**) indicate significant difference at the $P < 0.01$ level.

Table 3
Association analysis of single SNPs associated with V. anguillarum-resistance in 18-R and 18-S.

code	Location	Genotype	Count (frequence)		ChiSq genotype	ChiSqAllele	*P value*	
			18-S	18-R			ProbGenotype	ProbAllele
1	102	CC	23(0.657)	13(0.371)	6.19	8.914	0.045*	0.003**
		CT	7(0.200)	10(0.286)				
		TT	5(0.143)	12(0.343)				
7	2530	GG	7(0.200)	16(0.457)	6.522	9.287	0.038*	0.002**
		GA	10(0.286)	10(0.286)				
		AA	18(0.514)	9(0.257)				
9	3027	CC	20(0.571)	18(0.514)	8.915	3.963	0.012*	0.047*
		CT	13(0.371)	6(0.171)				
		TT	2(0.057)	11(0.314)				
10	3060	CC	14(0.400)	3(0.086)	11.695	4.286	0.002**	0.038*
		CT	6(0.171)	16(0.457)				
		TT	15(0.429)	16(0.457)				

Superscript (*) and (**) indicate significant difference at the $P < 0.05$ and $P < 0.01$ level, respectively.

Table 4
The frequencies of different haplotypes in 18-R and 18-S.

Variables	Haplotype	Frequency			Chi square values	*P value*	OR (95%CI)
		All	18-S	18-R			
Hap1	CC	0.385	0.455	0.314	3.473	0.06	0.519 (0.259, 1.038)
Hap2	TT	0.306	0.212	0.4	5.296	0.02*	2.384 (1.128, 5.039)

OR: odds ratio; CI: 95% percent confidence interval; Superscript (*) indicate significant difference at the $P < 0.05$ level.

invaded in the body. Collectively, all the results are implications of their roles in innate immunity which in turn suggest the general hypothesis about role of PIK3CA in host defense.

Previous studies have indicated that the PI3K/AKT pathway is activated or modulated in mammalians after virus infection [37,38]. The mRNA levels of catalytic subunit p110α increased 2–3 fold after WNV infection [38]. Aiming to determine whether *Sm*PIK3CA genes are involved in *V. anguillarum* resistance responses in turbot, we examined the amount of *Sm*PIK3CAs transcripts. The results showed that *Sm*PIK3CAa and *Sm*PIK3CA-like genes were elevated by 2–4 folds after bacterial infection, suggesting their involvement in disease responses. However, the peak time (1–6 h) of *Sm*PIK3CA-like was quicker than *Sm*PIK3CAa (6–12 h) in four tissues (Fig. 5). Although the transcript level was modest in most cases, the up-regulated expression can still be important considering the signal transduction functions of PI3KCAs.

Expression analysis in resistance group and susceptible group also provided evidence that the *Sm*PIK3CA genes are involved in the immune response after *V. anguillarum* challenge. The transcript levels of *Sm*PIK3CAa and *Sm*PIK3CA-like elevated in resistance individuals than in susceptible individuals in liver, spleen, kidney, gill and blood after infection. Similar with the previous situations, no significant was observed in both groups in the expression of *Sm*PIK3CAb, suggesting that *Sm*PIK3CAb has functional differentiation with *Sm*PIK3CAa and *Sm*PIK3CA-like. Future experimentation is warranted to confirm and validate the potential role of *Sm*PIK3CAb in other aspects.

Since *Sm*PIK3CA-like participates in the immune response of turbot, screening of resistance associated SNPs in this gene adds to the genetic markers that may be used for the selective breeding of turbot. In human cancers, high prevalence of PIK3CA mutations has been detected in exon 9 and exon 20 [39,40]. In the present study, based on groups with different levels of *V. anguillarum* resistance, four SNPs in exon region were identified as *V. anguillarum* resistance-related SNPs. Among the four SNPs, only 2530 (Asparticacid > Asparagine) produced amino acid variation. Any changes in CDS sequence and chemistry, even a point mutation, may induce a change in the secondary structures of protein which is reflected in the functions [41]. Besides, the catalytic subunit of PIK3CA (p110α) is essential for cell proliferation and inflammation response [29,42]. Three SNPs were located in the catalytic domain except SNP 102, implying a potential role in the changes of PIK3CA function. Hence, the expression levels of *Sm*PIK3CA-like could be adjusted to the genotypes of SNPs and further affect the *V. anguillarum* resistance in turbot. Moreover, SNPs usually to influence protein function with other SNPs in combination. It is an effective way to identify disease-associated genes by observe the particular combination of alleles in populations with different resistant levels [43]. In this study, a protective and a risk haplotype associated with *V. anguillarum* resistance were detected.

We verified the four SNPs and two haplotypes in population 18 which has independent genetic backgrounds with population 17. As expected, the genotype frequencies or allele frequencies of four identified SNPs also exhibited significant differences in group 18-S and 18-R. Hap2 (TT) also revealed a higher frequency in resistant group (18-R) than in the susceptible group (18-S). Taken all, the four SNPs together with Hap2 were confirmed and could be used as selective markers in *V. anguillarum* resistance breeding.

5. Conclusions

In summary, we identified and characterized three PIK3CA paralogs from *S. maximus* and their tissue expression profiles after infections with *V. anguillarum* assayed, representing the first analysis of PI3KCA genes among teleosts. Of the three PIK3CA genes, unlike *Sm*PIK3CAb, *Sm*PIK3CAa and *Sm*PIK3CA-like were determined to be differentially expressed after *V. anguillarum* infection, showing the evolution diversity in immune responses. In addition, we also detected and verified the SNPs and haplotypes associated with *V. anguillarum* resistance in *Sm*PIK3CA-like. Therefore, the duplicated PIK3CA-like genes probable play potential roles in innate immune defense against pathogenic agent invasions in *S. maximus*. This study provides novel insights into the turbot PIK3CA gene and open doors to further functional studies in PI3K family in teleost.

Conflicts of interest

The authors declare that they have no competing interests.

Acknowledgments

This study was supported by The Scientific and Technological Innovation Project from Laboratory for Marine Fisheries and Aquaculture, Qingdao National Laboratory for Marine Science and Technology (2015ASKJ02).

Appendix A. Supplementary data

Supplementary data to this article can be found online at https://doi.org/10.1016/j.fsi.2019.06.035.

References

[1] A.R. Saltiel, C.R. Kahn, Insulin signalling and the regulation of glucose and lipid metabolism, Nature 414 (6865) (2001) 799–806.
[2] A. Nobukazu, H. Tanenori, F. Aizo, J.A. Swanson, Phosphoinositide-3-kinase-independent contractile activities associated with Fcgamma-receptor-mediated phagocytosis and macropinocytosis in macrophages, J. Cell Sci. 116 (2) (2003) 247.
[3] J.R. Kong, W. Wei, Q.J. Liang, X.L. Qiao, H. Kang, Y. Liu, W.N. Wang, Identifying the function of LvPI3K during the pathogenic infection of *Litopenaeus vannamei* by *Vibrio alginolyticus*, Fish Shellfish Immunol. 76 (2018) 355–367.
[4] M.Q. Zhuo, Y.X. Pan, K. Wu, Y.H. Xu, Z. Luo, Characterization and mechanism of phosphoinositide 3-kinases (PI3Ks) members in insulin-induced changes of protein metabolism in yellow catfish *Pelteobagrus fulvidraco*, J. Gen. Comp. Endocrinol. 247 (2017) 34–45.
[5] K.D. Courtney, R.B. Corcoran, J.A. Engelman, The PI3K pathway as drug target in human cancer, J. Clin. Oncol. : Off. J. Am. Soc. Clin. Oncol. 28 (6) (2010) 1075–1083.
[6] M.D. Goncalves, B.D. Hopkins, L.C. Cantley, Phosphatidylinositol 3-kinase, growth disorders, and cancer, N. Engl. J. Med. 379 (21) (2018) 2052–2062.
[7] Y. Samuels, T. Waldman, Oncogenic mutations of PIK3CA in human cancers, J. Cell Cycle 3 (10) (2004) 1221–1224.
[8] P. Hu, A. Mondino, E.Y. Skolnik, J. Schlessinger, Cloning of a novel, ubiquitously expressed human phosphatidylinositol 3-kinase and identification of its binding site on p85, J. Mol. Cell Biol. 13 (12) (1993) 7677–7688.
[9] J.J. Zhao, H. Cheng, S. Jia, L. Wang, O.V. Gjoerup, A. Mikami, T.M. Roberts, The p110 alpha isoform of PI3K is essential for proper growth factor signaling and oncogenic transformation, Proc. Natl. Acad. Sci. Unit. States Am. 103 (44) (2006) 16296–16300.
[10] H.W. Chang, M. Aoki, D. Fruman, K.R. Auger, A. Bellacosa, P.N. Tsichlis, L.C. Cantley, T.M. Roberts, P.K. Vogt, Transformation of chicken cells by the gene encoding the catalytic subunit of PI 3-kinase, Science 276 (5320) (1997) 1848–1850.
[11] Z. Li, J. Yao, Y. Xie, X. Geng, Z. Liu, Phosphoinositide 3-kinase family in channel catfish and their regulated expression after bacterial infection, Fish Shellfish Immunol. 49 (2016) 364–373.
[12] Z. Li, X. Liu, J. Liu, K. Zhang, H. Yu, Y. He, X. Wang, J. Qi, Z. Wang, Q. Zhang, Transcriptome profiling based on protein-protein interaction networks provides a core set of genes for understanding blood immune response mechanisms against Edwardsiella tarda infection in Japanese flounder (*Paralichthys olivaceus*), Dev. Comp. Immunol. 78 (2018) 100–113.
[13] W. Wang, Y. Hu, Y. Ma, L. Xu, J. Guan, J. Kong, High-density genetic linkage mapping in turbot (*Scophthalmus maximus L.*) based on SNP markers and major sex- and growth-related regions detection, PLoS One 10 (3) (2015) e0120410.
[14] X. Liu, H. Zhang, Y. Gao, Y. Zhang, H. Wu, Y. Zhang, Efficacy of chitosan oligosaccharide as aquatic adjuvant administrated with a formalin-inactivated *Vibrio anguillarum* vaccine, Fish Shellfish Immunol. 47 (2) (2015) 855–860.
[15] X. Liu, H. Zhang, C. Jiao, Q. Liu, Y. Zhang, J. Xiao, Flagellin enhances the immunoprotection of formalin-inactivated Edwardsiella tarda vaccine in turbot, Vaccine 35 (2) (2017) 369–374.
[16] L. Zou, B. Liu, The polymorphisms of a MIF gene and their association with Vibrio resistance in the clam *Meretrix meretrix*, Dev. Comp. Immunol. 62 (2016) 116–126.
[17] J. Liu, N. Zhou, R. Fu, D. Cao, Y. Si, A. Li, H. Zhao, Q. Zhang, H. Yu, The polymorphism of chicken-type lysozyme gene in Japanese flounder (*Paralichthys olivaceus*) and its association with resistance/susceptibility to *Listonella anguillarum*, Fish Shellfish Immunol. 66 (2017) 43–49.
[18] D. Tan, L. Gram, M. Middelboe, Vibriophages and their interactions with the fish pathogen *Vibrio anguillarum*, Appl. Environ. Microbiol. 80 (10) (2014) 3128–3140.
[19] K. Zhang, M. Han, Y. Liu, X. Lin, X. Liu, H. Zhu, Y. He, Q. Zhang, J. Liu, Whole-genome resequencing from bulked-segregant analysis reveals gene set based association analyses for the *Vibrio anguillarum* resistance of turbot (*Scophthalmus maximus*), Fish Shellfish Immunol. 88 (2019) 76–83.
[20] T.M.J. Sambrook, E.F. Fritsch, Molecular cloning: a laboratory manual, 33 (1) (1982).
[21] A. Figueras, D. Robledo, A. Corvelo, M. Hermida, P. Pereiro, J.A. Rubiolo, J. Gomez-Garrido, L. Carrete, X. Bello, M. Gut, I.G. Gut, M. Marcet-Houben, G. Forn-Cuni, B. Galan, J.L. Garcia, J.L. Abal-Fabeiro, B.G. Pardo, X. Taboada, C. Fernandez, A. Vlasova, A. Hermoso-Pulido, R. Guigo, J.A. Alvarez-Dios, A. Gomez-Tato, A. Vinas, X. Maside, T. Gabaldon, B. Novoa, C. Bouza, T. Alioto, P. Martinez, Whole genome sequencing of turbot (*Scophthalmus maximus; Pleuronectiformes*): a fish adapted to demersal life, DNA Res. 23 (3) (2016) 181–192.
[22] A.-Y. Guo, B. Hu, G. Gao, H. Zhang, J. Luo, J. Jin, GSDS 2.0: an upgraded gene feature visualization server, Bioinformatics 31 (8) (2014) 1296–1297.
[23] R. Fredrik, J.P. Huelsenbeck, MrBayes 3: Bayesian phylogenetic inference under mixed models, Bioinformatics 19 (12) (2003) 1572–1574.
[24] A. Louis, N.T. Nguyen, M. Muffato, C.H. Roest, Genomicus update 2015: KaryoView and MatrixView provide a genome-wide perspective to multispecies comparative genomics, Nucleic Acids Res. 43 (Database issue) (2015) 682–689.
[25] K.J. Livak, T.D. Schmittgen, Analysis of relative gene expression data using real-time quantitative PCR and the 2(-Delta Delta C(T)) method, Methods 25 (4) (2001) 402–408.
[26] L. Wang, P. Liu, S. Huang, B. Ye, E. Chua, Z.Y. Wan, G.H. Yue, Genome-wide association study identifies loci associated with resistance to viral nervous necrosis disease in Asian seabass, Mar. Biotechnol. (NY) 19 (3) (2017) 255–265.
[27] Y.Y. Shi, L. He, SHEsis, a powerful software platform for analyses of linkage disequilibrium, haplotype construction, and genetic association at polymorphism loci, Cell Res. 15 (2) (2005) 97–98.
[28] J.A. Engelman, J. Luo, L.C. Cantley, The evolution of phosphatidylinositol 3-kinases as regulators of growth and metabolism, Nat. Rev. Genet. 7 (8) (2006) 606–619.
[29] P. Günzl, G. Schabbauer, Recent advances in the genetic analysis of PTEN and PI3K innate immune properties, Immunobiology 213 (9–10) (2008) 759–765.
[30] K. Hazeki, K. Nigorikawa, O. Hazeki, Role of phosphoinositide 3-kinase in innate immunity, Biol. Pharmaceut. Bull. 30 (9) (2007) 1617–1623.
[31] I.D. Hiles, M. Otsu, S. Volinia, M.J. Fry, I. Gout, R. Dhand, G. Panayotou, F. Ruiz-Larrea, A. Thompson, N.F. Totty, Phosphatidylinositol 3-kinase: structure and expression of the 110 kd catalytic subunit, Cell 70 (3) (1992) 419–429.
[32] A. Angel, C. Julian, F. Allyse, F. Quenton, J.H. Postlethwait, Genome evolution and meiotic maps by massively parallel DNA sequencing: spotted gar, an outgroup for the teleost genome duplication, J. Genet. 188 (4) (2011) 799–808.
[33] C.L. Carpenter, B.C. Duckworth, K.R. Auger, B. Cohen, B.S. Schaffhausen, L.C. Cantley, Purification and characterization of phosphoinositide 3-kinase from rat liver, J. Biol. Chem. 265 (32) (1990) 19704.
[34] F. Wang, S. Xiao, Y. Zhang, Y. Zhang, Y. Liu, Y. Yan, Z. Xiang, Z. Yu, ChAkt1 involvement in orchestrating the immune and heat shock responses in *Crassostrea hongkongensis*: molecular cloning and functional characterization, Fish Shellfish Immunol. 47 (2) (2015) 1015–1023.
[35] S.W. Luo, W.N. Wang, R.C. Xie, F.X. Xie, J.R. Kong, Y.C. Xiao, D. Huang, Z.M. Sun, Y. Liu, C. Wang, Molecular cloning and characterization of PTEN in the orange-spotted grouper (*Epinephelus coioides*), Fish Shellfish Immunol. 58 (2016) 686–700.
[36] M.O. Hagen, B.A. Katzenback, M.D. Islam, M. Gamal El-Din, M. Belosevic, The analysis of goldfish (*Carassius auratus L.*) innate immune responses after acute and subchronic exposures to oil sands process-affected water, Toxicol. Sci. : Off. J. Soc. Toxicol. 138 (1) (2014) 59–68.
[37] M. Tokuyama, C. Lorin, F. Delebecque, H. Jung, D.H. Raulet, L. Coscoy, Expression of the RAE-1 family of stimulatory NK-cell ligands requires activation of the PI3K pathway during viral infection and transformation, PLoS Pathog. 7 (9) (2011) e1002265.
[38] L. Wang, L. Yang, E. Fikrig, P. Wang, An essential role of PI3K in the control of West Nile virus infection, Sci. Rep. 7 (1) (2017) 3724.
[39] S. Mjos, H.M.J. Werner, E. Birkeland, F. Holst, A. Berg, M.K. Halle, I.L. Tangen, K. Kusonmano, K.K. Mauland, A.M. Oyan, K.H. Kalland, A.E. Lewis, G.B. Mills, C. Krakstad, J. Trovik, H.B. Salvesen, E.A. Hoivik, PIK3CA exon9 mutations associate with reduced survival, and are highly concordant between matching primary tumors and metastases in endometrial cancer, Sci. Rep. 7 (1) (2017) 10240.
[40] M. Gymnopoulos, M.A. Elsliger, P.K. Vogt, Rare cancer-specific mutations in PIK3CA show gain of function, Proc. Natl. Acad. Sci. U.S.A. 104 (13) (2007) 5569–5574.
[41] N. Rubin, E. Perugia, S.G. Wolf, E. Klein, M. Fridkin, L. Addadi, Relation between serum amyloid A truncated peptides and their suprastructure chirality, J. Am. Chem. Soc. 132 (12) (2010) 4242–4248.
[42] C. Saponaro, A. Cianciulli, R. Calvello, T. Dragone, F. Iacobazzi, M.A. Panaro, The PI3K/Akt pathway is required for LPS activation of microglial cells, Immunopharmacol. Immunotoxicol. 34 (5) (2012) 858–865.
[43] S.B. Gabriel, S.F. Schaffner, H. Nguyen, J.M. Moore, J. Roy, B. Blumenstiel, J. Higgins, M. DeFelice, A. Lochner, M. Faggart, S.N. Liu-Cordero, C. Rotimi, A. Adeyemo, R. Cooper, R. Ward, E.S. Lander, M.J. Daly, D. Altshuler, The structure of haplotype blocks in the human genome, Science 296 (5576) (2002) 2225–2229.